Arthritis & Rheumatology
Vol. 77, No. 6, June 2025, pp 740–749
DOI 10.1002/art.43094

American College of Rheumatology
Empowering Rheumatology Professionals

BRIEF REPORT

Disturbed Spatial WNT Activation—A Potential Driver of the Reticularized Skin Phenotype in Systemic Sclerosis

Sara Chenguiti Fakhouri,[1] Honglin Zhu,[2] Yi-Nan Li,[3] Moritz Ronicke,[4] Aleix Rius Rigau,[5] Clara Dees,[6] Laura Konstantinidis,[7] Ralf Schmid,[8] Alexandru-Emil Matei,[9] Markus Eckstein,[10] Carol Geppert,[11] Ingo Ludolph,[12] Alexander Kreuter,[13] Michael Sticherling,[14] Carola Berking,[15] Raymund E. Horch,[16] Georg Schett,[17] Jörg H. W. Distler,[18] and Christina Bergmann[19]

Objective. Little is known on the mechanisms necessary to maintain the physiologic adult human skin integrity. This study aims to quantitatively describe anatomic changes in systemic sclerosis (SSc)–skin compared with controls and investigate the underlying mechanisms.

Methods. Skin morphology was histologically assessed in 23 patients with SSc, 18 controls, and 15 patients with hypertrophic scars. Spatial WNT/β-catenin-activation was analyzed by RNAscope and immunofluorescence staining. Enrichment of reticular marker genes in predefined fibroblast subpopulations was done using Gene Ontology (GO) enrichment and gene set enrichment analysis.

Results. SSc skin showed a decrease in number ($P < 0.0001$/$P = 0.0004$), area ($P < 0.0001$), and height ($P < 0.0001$) of papillae compared with controls and hypertrophic scars, respectively. The expression of papillary/reticular marker genes shifted toward a reticular expression profile in SSc. On the level of previously defined fibroblast populations, the increase of reticular marker genes was particularly pronounced in the PI16+ and SFRP4+ populations ($P <$ 0.0001, respectively). Mechanistically, the expression of the WNT/β-catenin target *AXIN2* and the number of fibroblasts with nuclear β-catenin-staining-pattern increased in the papillary compared with the reticular dermis in healthy skin. This polarization was lost in SSc with a two-fold increase in β-catenin-positive fibroblasts and *AXIN2*-expressing fibroblasts throughout the dermis ($P = 0.0095$). Enrichment of genes related to WNT/β-catenin-regulation was found in the PI16+ population that also relocates from the reticular to the papillary dermis in SSc.

Conclusion. We demonstrate an association of the "reticularized" skin phenotype in SSc with a profound loss of physiologic spatial WNT/β-catenin-activation. Rescuing the spatial WNT/β-catenin-activation might help restore the physiologic skin organization in future therapeutic approaches of fibrosing disorders.

INTRODUCTION

Systemic sclerosis (SSc) is a chronic connective tissue disorder that results in progressive fibrotic tissue changes of the skin and inner organs. The skin is affected in almost all patients starting from the distal extremities (sclerodactyly) expanding to the proximal parts of the body during the course of the disease.[1] Skin fibrosis is a major cause of daily life impairment,[2] and the extent

This work was completed in the context of the doctoral thesis of Sara Chenguiti Fakhouri.

Supported by the German Research Foundation (grants BE 7036/2-1 (C. Bergmann, BE 7036/5-1 (C Bergmann, DI 1537/17-1 (JHW Distler), DI 1537/20-1 (JHW Distler), DI 1537/22-1 (JHW Distler), and DI 1537/23-1 (JHW Distler), the SFB (Sonderforschungsbereiche) CRC (Collaborative Research Center) 1181 (project A01 and C01 (G Schett, JHW Distler), the NOTICE Clinician Scientist Program of the German Research Association (grant RA 2506/7-21 to Drs Ronicke, Berking, and Bergmann), the ELAN (Erlanger Anschubsfinanzierung) Erlangen (grant 21-11-09-1 to C Bergmann), the Clinician Scientist Program of IZKF (Interdisziplinäre Zentrum für Klinische Forschung) Erlangen (C Bergmann), and the Bundesministerium für Bildung und Forschung (iIMMUNE_ACS program, project 01EO2105, C Bergmann).

[1]Sara Chenguiti Fakhouri, MSc: Department of Internal Medicine 3 - Rheumatology and Clinical Immunology, Friedrich-Alexander-University (FAU) Erlangen-Nürnberg and Uniklinikum Erlangen, Erlangen, Germany, and Deutsches Zentrum Immuntherapie (DZI), FAU Erlangen-Nürnberg and Uniklinikum Erlangen, Erlangen, Germany; [2]Honglin Zhu, MD: Department of Rheumatology and Immunology, Xiangya Hospital, Central South University, Changsha, Hunan, People's Republic of China; [3]Yi-Nan Li, PhD: Department of Rheumatology, University Hospital Düsseldorf, Medical Faculty of Heinrich Heine University, Düsseldorf, Germany, and Hiller Research Center, University Hospital Düsseldorf, Medical Faculty of Heinrich Heine University, Düsseldorf, Germany; [4]Moritz Ronicke, MD: Deutsches Zentrum Immuntherapie (DZI), FAU Erlangen-Nürnberg and Uniklinikum Erlangen, Erlangen, Germany, and Department of Dermatology, Friedrich-Alexander-University (FAU) Erlangen-Nürnberg and Uniklinikum Erlangen, Erlangen, Germany; [5]Aleix Rius Rigau, PhD: Department of Internal Medicine 3 - Rheumatology and Clinical Immunology, Friedrich-Alexander-University (FAU) Erlangen-Nürnberg and Uniklinikum Erlangen, Erlangen, Germany, and Deutsches Zentrum Immuntherapie (DZI), FAU Erlangen-Nürnberg and Uniklinikum Erlangen, Erlangen, Germany; [6]Clara Dees, PhD: Department of Internal Medicine 3 - Rheumatology and Clinical Immunology, Friedrich-

of skin involvement is recognized as risk factor for the progression of organ fibrosis.[3]

Healthy human skin forms the interface between the body and the environment and is characterized by a polarized, layered structure including the epidermis, the papillary and reticular dermis and the subcutaneous fat tissue.[4] The papillary dermis is composed of loose collagen bundles surrounding blood vessels and nerve endings, whereas the reticular dermis is characterized by coarse collagen bundles.[5] This physiologic skin structure is disrupted in SSc: the deregulation of fibroblasts and increased differentiation into myofibroblasts results in the exaggerated deposition of collagen-rich extracellular matrix throughout the dermis along with morphologic changes such as flattening of the rete ridges and loss of functional intradermal structures and skin appendices.[6,7] Previous studies have described a correlation between histologic changes such as the hyalinized collagen score and the extent of local skin involvement as assessed by the modified Rodan skin score.[7,8]

The mechanisms that are required to maintain the physiologic layered organization of healthy skin are largely unknown. Evidence from rodent models of skin morphogenesis suggests that spatial activation of WNT/β-catenin signaling at the cellular and tissue level plays a central role in three-dimensional skin patterning.[9] WNT/β-catenin signaling has been characterized as central profibrotic regulator in fibrosing disorders by several groups.[10–15] –15 Activation occurs by overexpression of certain WNT proteins and by reduced expression of the endogenous WNT antagonist DKK1 in the skin.[13] However, the spatial resolution of WNT activators and antagonists in adult human skin has not been described. Moreover, the mechanisms that maintain the polarized structure of the skin in adults have barely been elucidated. Here we aimed to characterize the histopathologic changes in SSc skin, investigate the spatial regulation of WNT/β-catenin signaling in normal human skin compared with SSc skin, and correlate changes in spatial WNT/β-catenin signaling with histopathological characteristics in SSc.

PATIENTS AND METHODS

Patients. Skin biopsies from 23 patients with SSc and 18 healthy volunteers were used. All patients with SSc fulfilled the 2013 American College of Rheumatology/EULAR criteria for SSc. Twenty-two patients had limited cutaneous SSc and 41 were classified as diffuse cutaneous SSc according to the LeRoy classification.[16] Skin biopsies from patients with SSc were taken from involved skin on the forearm. In 18 patients with SSc, skin biopsies were additionally taken from a clinically noninvolved skin area at the back. Eighteen patients were female, and five were male. The median age of patients with SSc was 55 years (range 41–69 years), and the median disease duration was 5 years (range 1–12 years). Control skin samples from 18 healthy individuals who underwent either orthopedic or plastic surgery were included. In addition, 15 samples of patients with hypertrophic scars were analyzed. The diagnosis of hypertrophic scars was based on the clinical judgment of two experienced dermatologists in conjunction with the histopathologic findings. The collection of biology samples and their analysis in context with clinical information were approved by the ethics committee of the Medical Faculty of the University of Erlangen-Nuremberg. All patients and

Alexander-University (FAU) Erlangen-Nürnberg and Uniklinikum Erlangen, Erlangen, Germany, and Deutsches Zentrum Immuntherapie (DZI), FAU Erlangen-Nürnberg and Uniklinikum Erlangen, Erlangen, Germany; [7]Laura Konstantinidis: Department of Internal Medicine 3 - Rheumatology and Clinical Immunology, Friedrich-Alexander-University (FAU) Erlangen-Nürnberg and Uniklinikum Erlangen, Erlangen, Germany, and Deutsches Zentrum Immuntherapie (DZI), FAU Erlangen-Nürnberg and Uniklinikum Erlangen, Erlangen, Germany; [8]Rafael Schmid, PhD: Department of Plastic and Hand Surgery, Laboratory for Tissue Engineering and Regenerative Medicine, University Hospital Erlangen, Friedrich Alexander University Erlangen-Nürnberg FAU, Erlangen, Germany; [9]Alexandru-Emil Matei, MD: Department of Rheumatology, University Hospital Düsseldorf, Medical Faculty of Heinrich Heine University, Düsseldorf, Germany, and Hiller Research Center, University Hospital Düsseldorf, Medical Faculty of Heinrich Heine University, Düsseldorf, Germany; Fraunhofer Institute for Translational Medicine and Pharmacology ITMP, and Fraunhofer Cluster of Excellence for Immune Mediated Diseases CIMD, Frankfurt am Main, Germany; [10]Markus Eckstein, MD: Department of Pathology, Friedrich-Alexander-University (FAU) Erlangen-Nürnberg and Uniklinikum Erlangen, Erlangen, Germany; [11]Carol Geppert, MD: Department of Pathology, Friedrich-Alexander-University (FAU) Erlangen-Nürnberg and Uniklinikum Erlangen, Erlangen, Germany; [12]Ingo Ludolph, MD: Department of Plastic and Hand Surgery, Laboratory for Tissue Engineering and Regenerative Medicine, University Hospital Erlangen, Friedrich Alexander University Erlangen-Nürnberg FAU, Erlangen, Germany; [13]Alexander Kreuter, MD: Department of Dermatology, Venereology, and Allergology, HELIOS St. Elisabeth Hospital Oberhausen, Oberhausen, Germany; [14]Michael Sticherling, MD: Deutsches Zentrum Immuntherapie (DZI), FAU Erlangen-Nürnberg and Uniklinikum Erlangen, Erlangen, Germany, and Department of Dermatology, Friedrich-Alexander-University (FAU) Erlangen-Nürnberg and Uniklinikum Erlangen, Erlangen, Germany; [15]Carola Berking, MD: Deutsches Zentrum Immuntherapie (DZI), FAU Erlangen-Nürnberg and Uniklinikum Erlangen, Erlangen, Germany, and Department of Dermatology, Friedrich-Alexander-University (FAU) Erlangen-Nürnberg and Uniklinikum Erlangen, Erlangen, Germany; [16]Raymund E. Horch, MD: Department of Plastic and Hand Surgery, Laboratory for Tissue Engineering and Regenerative Medicine, University Hospital Erlangen, Friedrich Alexander University Erlangen-Nürnberg FAU, Erlangen, Germany; [17]Georg Schett, MD: Department of Internal Medicine 3 - Rheumatology and Clinical Immunology, Friedrich-Alexander-University (FAU) Erlangen-Nürnberg and Uniklinikum Erlangen, Erlangen, Germany, and Deutsches Zentrum Immuntherapie (DZI), FAU Erlangen-Nürnberg and Uniklinikum Erlangen, Erlangen, Germany; [18]Jörg H. W. Distler, MD: Department of Rheumatology, University Hospital Düsseldorf, Medical Faculty of Heinrich Heine University, Düsseldorf, Germany, and Hiller Research Center, University Hospital Düsseldorf, Medical Faculty of Heinrich Heine University, Düsseldorf, Germany; Fraunhofer Institute for Translational Medicine and Pharmacology ITMP, and Fraunhofer Cluster of Excellence for Immune Mediated Diseases CIMD, Frankfurt am Main, Germany; [19]Christina Bergmann, MD: Department of Internal Medicine 3 - Rheumatology and Clinical Immunology, Friedrich-Alexander-University (FAU) Erlangen-Nürnberg and Uniklinikum Erlangen, Erlangen, Germany.

Additional supplementary information cited in this article can be found online in the Supporting Information section (https://acrjournals.onlinelibrary.wiley.com/doi/10.1002/art.43094).

Author disclosures are available at https://onlinelibrary.wiley.com/doi/10.1002/art.43094.

Address correspondence via email to Christina Bergmann, MD, at christina.bergmann@uk-erlangen.de.

Submitted for publication January 10, 2024; accepted in revised form December 5, 2024.

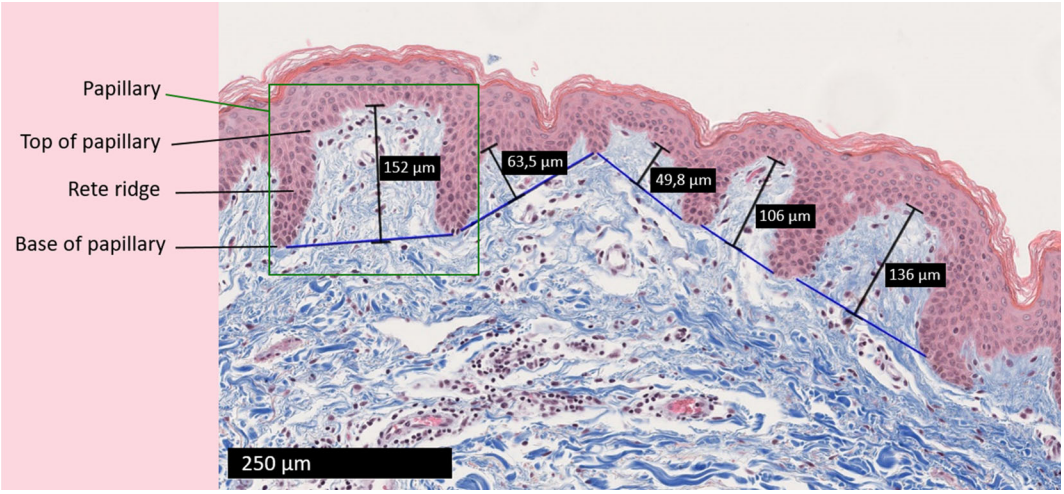

Figure 1. Visualization of papillary measurements.

control individuals signed an informed consent form approved by the local review board.

Histologic analyses. For visualization and quantification of dermal papillae, trichrome staining of the skin sections was used as described previously.[17–19] Pictures were taken at 200-fold magnification with a Nanozoomer S60v2MD slide scanner (Hamamatsu Photonics). Papillae numbers per mm, papillae heights (defined as the distance between the base and the top of the papillae as demonstrated in Figure 1) and papillae areas were quantified at five different sites in one skin section from each patient in a blinded manner using the NDPView2 software (Hamamatsu Photonics).

Collagen fiber alignment (from 0° to 180°) and alignment coefficients were measured using Curvealign V4.0 Beta (MATLAB). Three regions of interest of 0.02 mm^2 were selected in the reticular dermis of each trichrome-stained skin section. The coefficient of alignment was calculated for all the collagen fibers within each region of interest using the Computed Tomography–Fiber analysis method according to the developer's manual (https://eliceirilab.org/software/curvealign/). The alignment coefficient was calculated from zero (low parallelism between collagen fibers) to one (high parallelism between collagen fibers).

Immunofluorescence. Paraffin-embedded skin sections were fixed with 4% paraformaldehyde.[20] Epitope retrieval was performed using a heat-induced method; sections were incubated with preheated citrate buffer (10 mM sodium citrate, pH 6.0) and Tris-EDTA buffer (10 mM Tris, 1 mM EDTA, 0.05% Tween 20, pH 9.0). Sections were then blocked with phosphate buffered saline (PBS) supplemented with 2% Bovine serum albumin (BSA) and 5% horse serum. Primary antibodies were incubated overnight at 4°C. After washing, secondary antibodies were incubated for an hour at room temperature. Next, the sections were counterstained with 4´,6-diamidino-2-phenylindole (DAPI) (1:800, #sc-3598 Santa Cruz Biotechnology). Primary antibodies used were directed against β-catenin (1:250, #ab2365; abcam), prolyl-4-hydroxylase β (P4Hβ) (1:200, #ab2792; abcam), platelet derived growth factor α (PDGFRα) (1:200, #AF1062; R&D Systems), PI16 (1/200, #HPA043763; Atlas Antibodies), secreted frizzeled related protein 4 (SFRP4, 1:20, 15328-1-AP, Proteintech), Dickkopf-1 (1:100, #AF1096; R&D Systems), vimentin (1:1000, NBP1-97515; Novus Biologicals), Fibroblast activation protein α (FAP) (1:200, #AF3715; R&D Systems), CD90/Thy1 (1:250, #ab133350; abcam). Conjugated secondary antibodies (1:200, Alexa Fluor, Thermo Fisher Scientific) were used. Nuclei were stained with DAPI (1:800, #sc-3598, Santa Cruz Biotechnology). The staining was analyzed using a Nikon Eclipse 80i microscope (Nikon) and a BZ-X800 microscope (Keyence). Pictures were taken at 200-fold magnification. Borders of the papillary and reticular dermis were defined anatomically; we considered the superficial vascular plexus to be the limit between the papillary and reticular dermis.[21] Thus, the papillary dermis was defined by the dermal-epidermal junction and the superficial vascular plexus. The reticular dermis was defined by the superficial vascular plexus and the beginning of the subcutis. Semiquantitative quantification of β-catenin-, FAP-, CD90-, PI16-, and SFRP4-positive cells in the papillary and reticular dermis was performed at three different sites of one skin section from each patient or control individual, in a blinded manner, using the Nikon NIS-Element software platform (Nikon). The β-catenin fluorescence intensity in the papillary and reticular dermis was quantified at seven different sites in one skin section from each patient or control using the ImageJ software (NIH, version 1.46).

RNAscope assay. Spatial transcriptional activation of the WNT/β-catenin pathway was assessed through in situ

hybridization detection of *AXIN2* using an RNAscope Multiplex Fluorescent Kit V2 (Advanced Cell Diagnostics) combined with TSA Vivid Fluorophores (Bio-Techne) on paraffin-embedded, formalin-fixed skin sections according to the manufacturer's instructions. Briefly, formalin-fixed, paraffin-embedded skin sections are permeabilized to allow probe access to the target RNA. Probes are then hybridized to target RNA and labeled with fluorophores. Finally, the hybridization signal is amplified by sequentially binding amplifiers and labeled probes and nuclei were stained with DAPI. Quantification of *AXIN2*-positive cells in the papillary and reticular dermis was performed at three different sites of one skin section from each patient or control, in a blinded manner, using the Nikon NIS-Element software platform (Nikon). The *AXIN2* fluorescence intensity in the papillary and reticular dermis was quantified at four to seven different sites in one skin section from each patient or control using the ImageJ software (NIH, version 1.46).

Confocal microscopy and analysis. Confocal images of skin sections were acquired using a Leica Stellaris 8 confocal microscope (Leica Microsystems) at the Optical Imaging Center Erlangen. Pictures were taken at 630-fold magnification with a glycerol immersion lens and a resolution of 1024 × 1024 pixels. Stacks of images were acquired at 1 µm interval throughout the cells, in the papillary and the reticular dermis. The fluorescence intensity of the cytoplasmic and nuclear β-catenin was measured by creating a mask based on the fluorescent signal of the pan-fibroblast marker P4Hβ antibody (1:200, #ab2792; abcam) and DAPI (1:800, #sc-3598 Santa Cruz Biotechnology), respectively. To this end, the channel containing the DAPI nuclear marker was converted to a mask, which was applied to the β-catenin signal, and the fluorescence intensity analysis was performed by thresholding using the MorpholibJ plugin on the ImageJ software (NIH, version 1.46). The same procedure was conducted for cytoplasmic β-catenin with the pan-fibroblast marker P4Hβ signal.

Imaging mass cytometry staining and measurements. Imaging mass cytometry (IMC) was performed as described.[21] The antibodies were acquired preconjugated (Standard Biotools) or in purified preparations. All the purified antibodies were first validated by standard immunofluorescence staining. Purified antibodies were consequently conjugated to lanthanide metals using the Maxpar X8 antibody labeling kit (Standard Biotools) following the manufacturer's instructions. The full panel was revalidated in IMC, and all antibodies were titrated in IMC. Paraffin-embedded skin sections (5 µm) were deparaffinized with xylene for 30 minutes and rehydrated in a graded series of alcohol (ethanol:deionized water 100:0, 100:0, 90:10, and 80:20 for 5 minutes each). For epitope retrieval, the slides were incubated for 30 minutes in preheated Tris-EDTA buffer (10 mM Tris base, 1 mM EDTA, and 0.05% Tween 20, pH 9). After the slides were cooled, they were blocked with 2% BSA in PBS for one hour at room temperature. Samples were incubated overnight at 4°C with the antibody mix (in 0.5% BSA). Tissue samples were washed once in PBS-T (PBS and 0.2% Tween 20) and twice in PBS for five minutes each wash. DNA staining was performed with Iridium-Intercalator (125 µM) (Standard Biotools) 1/400 for five minutes at room temperature. Afterward, the samples were washed three times in PBS and once in deionized water for five minutes each. Finally, the tissue sections were dried and stored at room temperature.

The area to be ablated was chosen with a hematoxylin-eosin staining of a consecutive cut. The samples were acquired with the Hyperion Imaging System (Standard Biotools) coupled to a Helios mass cytometer (Standard Biotools) after daily calibration, tuning, and quality control. The laser ablation was done at a resolution of 1 μm^2 and a frequency of 200 Hz. All IMC data were stored as MCD and txt files.

IMC data analysis. First, the quality of the staining was checked with the software MCD viewer (Standard Biotools). The MCD files were converted to TIFF format and segmented into single cells using a publicly available analysis pipeline (https://zenodo.org/record/3841961). The single-cell data (mean expression of all pixels being the same cell and the spatial coordinates) were extracted as fcs and csv files, arcsinh normalized (cofactor 1), and rescaled between 0 and 1 with the R package Spectre.[21] The populations of interest were selected by manual gating and spatial reference using the FlowJo software (fibroblasts were defined as Ecadherin-CD45-CD31-; afterward skin fibroblast subsets were selected: fibroblast FAP+CD90+, FAP+CD90–, FAP-CD90+.). The spatial representation of the different cell populations was done with the R package Cytomapper.[22,23]

Gene set enrichment analyses. Gene set enrichment analyses (GSEA) were performed using the R packages clusterProfiler (3.18.0) and GSVA (V1.38.0). Reticular and papillary gene signature[24] scores in the Prospective Registry for Early Systemic Sclerosis (PRESS) cohort[25] (GSE130955) and the Genes versus Environment in Scleroderma Outcome Study (GENISOS) cohort (GSE58095)[26] were obtained through single-sample gene set enrichment analysis using gene lists from Solé-Boldo et al.[24] GSEA was used to analyze WNT3A-regulated gene signatures in relation to reticular and papillary marker genes,[24] the enrichment of reticular and papillary marker genes[24] in predefined fibroblast subsets,[27,28] and the enrichment of WNT3A-regulated genes in the PI16+/– fibroblast population.

Statistical analysis. All data are presented as median with interquartile range with individual datapoints displayed as dots. Comparisons between experimental groups were analyzed with nonparametric Mann-Whitney-U-test using GraphPad Prism 8.3.0. In analysis including multiple tests, the *P* value of each test

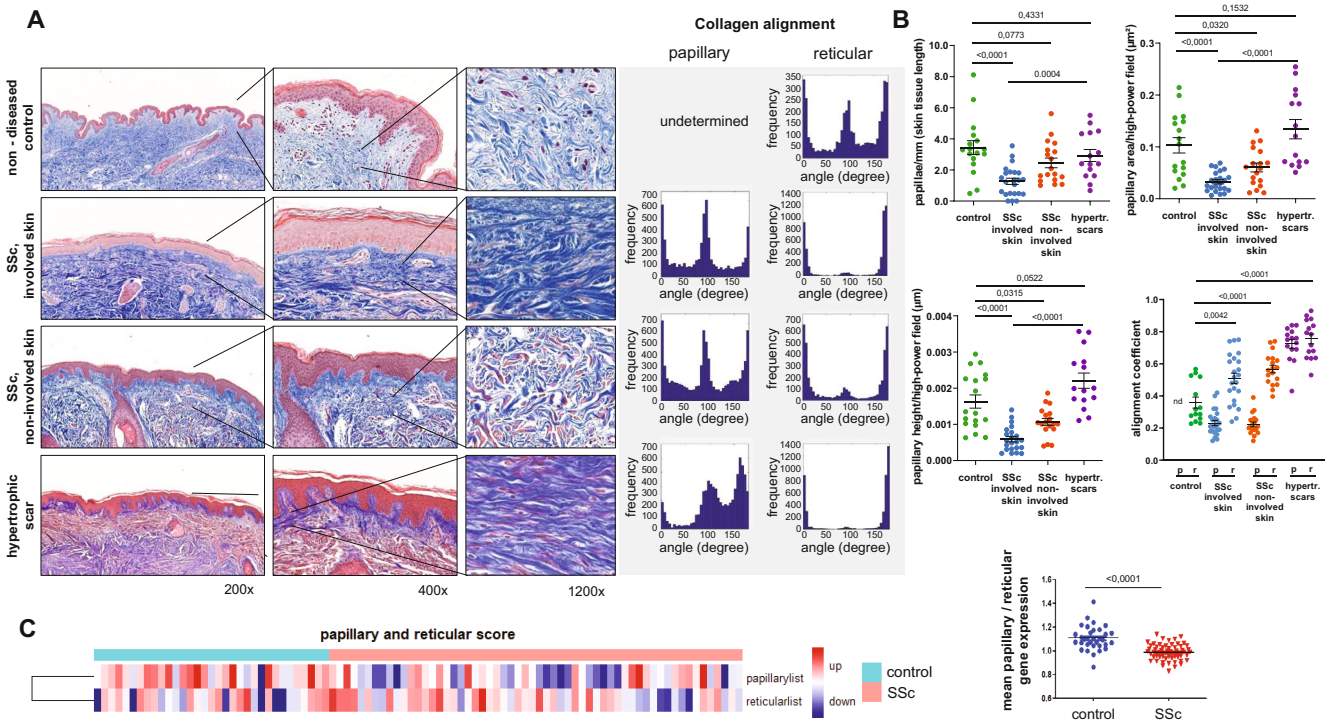

Figure 2. Morphology of the dermal papillae in SSc compared with nondiseased skin and hypertrophic scars. (A) Trichrome staining of skin sections of nondiseased control individuals (n = 18), involved (forearm) and noninvolved (back) skin of patients with SSc (n = 23), patients with hypertrophic scars (n = 15), and corresponding histograms representing collagen fiber orientation in angle frequency of individual collagen fibers. Representative images are shown at 200-, 400-, and 1,200-fold magnification. (B) Quantification of papillae/mm, papillary area/high-power field, papillary height/high-power field and collagen fiber alignment coefficient of skin sections of control individuals (n = 18), patients with SSc (n = 23), and patients with hypertrophic scars (n = 15) quantified from trichrome staining images. (C) Papillary and reticular gene scores in Prospective Registry for Early Systemic Sclerosis cohort (GSE130955) (Gene set list from Solé-Boldo et al[24]). Data are presented as median ± interquartile range. Statistical significance for each comparison was determined by Mann-Whitney U-test. $P < 0.0125$ was considered significant after Bonferroni correction. hypertr., hypertrophic; p, papillary; r, reticular; SSc, systemic sclerosis. Color figure can be viewed in the online issue, which is available at http://onlinelibrary.wiley.com/doi/10.1002/art.43094/abstract.

(p_i) was adjusted using the Bonferroni correction (pi = p/n, n = number of tests, p = overall significance level).

RESULTS

Assessment of structural changes in fibrotic skin in SSc compared with nondiseased control skin and hypertrophic scars. Quantitative assessments of changes in the papillary dermis in SSc have not been described so far. Here, we analyzed the number of papillae per millimeter, papillae length, and area in trichrome-stained skin sections of healthy individuals, involved skin of patients with SSc (forearm), clinically noninvolved skin of patients with SSc (back), and of patients with hypertrophic scars as a second type of fibrosing skin disorder. In SSc-involved skin, dermal papillae were markedly decreased in number, area, and height compared with controls (Figure 2A and B).

Noninvolved SSc skin showed higher papillary content (papillae per mm, papillae length and papillae area) compared with clinically involved skin in SSc (Figure 2A and B), albeit below the level of nondiseased controls. In contrast, number, area, and height of papillae in hypertrophic scars did not significantly differ from healthy controls, suggesting that papillary loss is a phenomenon specific to SSc rather than a general feature of fibrosing dermal disorders (Figure 2A and B). The papillae measurements including papillae number per mm, height, and area did not significantly differ between patients with limited cutaneous SSc (lcSSc) compared with diffuse cutaneous SSc (dcSSc) (Supplementary Figure 1).

As additional readout, we analyzed the orientation of collagen fibers using trichrome staining in skin sections of healthy donors, involved skin of patients with SSc, noninvolved skin of SSc, and hypertrophic scars. SSc skin and hypertrophic scar sections showed a higher alignment coefficient than healthy controls in the reticular dermis and a measurable alignment coefficient in the papillary dermis, consistent with the increased extracellular matrix deposition and the "reticularization" of the papillary dermis (Figure 2A and B). In healthy skin, the loose structure of the extracellular matrix in the papillary layer did not allow for a specific detection of individual collagen fibers and an alignment coefficient

could not be calculated. When comparing lcSSc and dcSSc skin sections, we measured similar levels of collagen alignment between the two subtypes, confirming a shared structural remodeling (Supplementary Figure 1).

To confirm these histologic observations with another approach, we compared published datasets of papillary and reticular marker genes[24] with differentially regulated genes in SSc compared with healthy controls described in the PRESS cohort.[25] Consistent with the morphologic changes, we observed that the expression of papillary versus reticular marker genes is shifted toward a reticular gene expression profile in SSc skin samples (Figure 2C). This is also reflected by the reduction of the ratio of mean papillary gene expression/mean reticular papillary gene expression in SSc compared with controls. Because the PRESS cohort mainly includes patients with early diffused disease and to confirm our results in another cohort dataset, we next analyzed the enrichment of papillary and reticular marker sets in a published dataset of the GENISOS cohort.[26] The GENISOS cohort includes patients with both lcSSc and dcSSc and with variable disease duration ranging from 0.5 to 20 years since the first onset of first non-Raynaud symptom. Analyzing the whole cohort, we observed a tendency of reduction of the papillary/reticular gene ratio, which was not significant (Supplementary Figure 2). Next, we analyzed patients with relatively low disease duration (≤4 years) and compared them with patients with a longer disease duration (>4 years). Similar to our results obtained in the PRESS cohort, we observed a significant reduction of papillary/reticular marker genes in patients with less than or equal to four years disease duration. The majority of patients in this subgroup suffered from dcSSc, and no significant difference was observed between lcSSc and dcSSc. Reduction of the papillary/reticular score was less pronounced in patients with longer disease duration (>4 years) and was not statistically significant (Supplementary Figure 2).

Altered spatial activation of WNT signaling in SSc compared with healthy controls. A tightly regulated spatial activation of WNT/β-catenin signaling has recently been described as a core requirement for physiologic skin morphogenesis in mice.[29] Moreover, WNT/β-catenin signaling has been described as a central profibrotic mediator.[10,30] We thus analyzed whether a spatial WNT/β-catenin activation is observed in adult healthy skin and might be perturbed in SSc. First, we analyzed whether WNT/β-catenin-dependent target genes (GSE120106) are enriched in the papillary and in the reticular part of healthy skin.[24] We observed an enrichment of WNT3A-regulated genes in papillary healthy skin, and a tendency toward negative enrichment in reticular gene sets (Supplementary Figure 3A). In contrast to WNT3A-regulated genes, WNT5A-regulated gene signatures as markers of noncanonical WNT signaling did not show

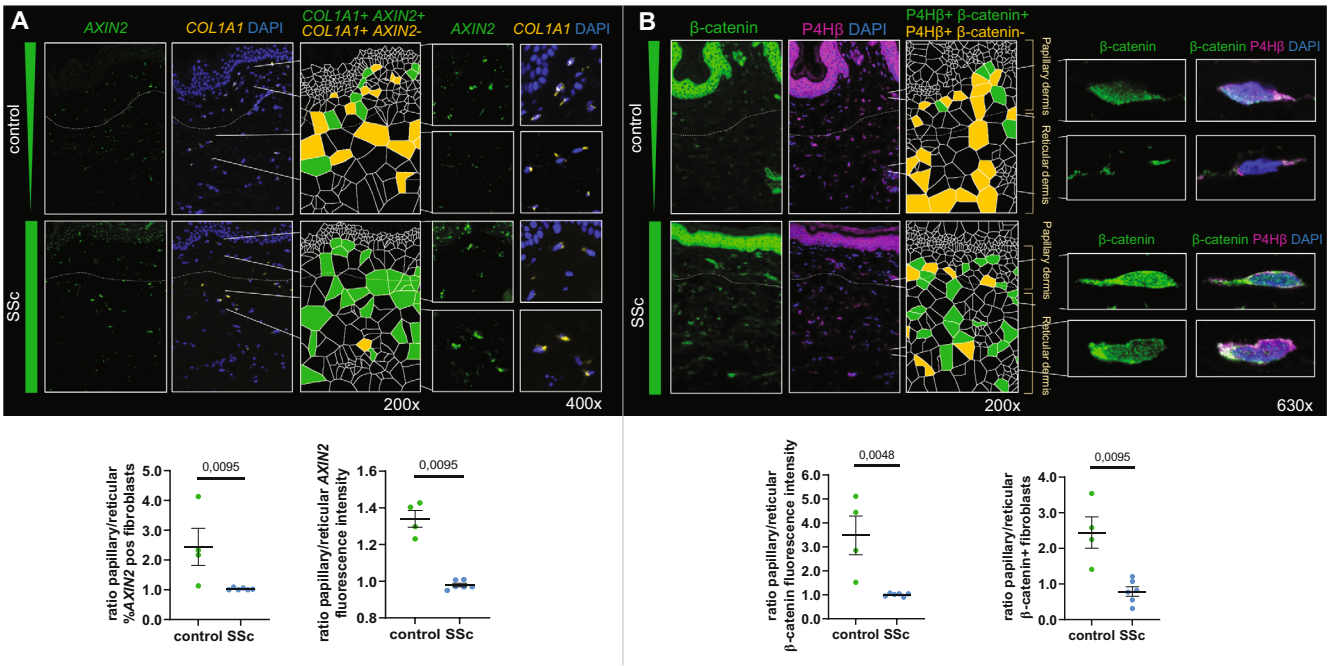

Figure 3. Spatial activation of WNT/β-catenin signaling in healthy and SSc skin. (A) RNAscope in situ hybridization images of *COL1A1* (orange) and *AXIN2* (green) on skin sections of healthy individuals and patients with SSc. Representative images are shown at 200- and 400-fold magnification. Quantification is shown as bar graph. (B) Immunofluorescence staining and confocal immunofluorescence microscopy for β-catenin (green) and the pan-fibroblast marker P4Hβ (magenta) of papillary and reticular fibroblasts from nondiseased control individuals (n = 4) and patients with SSc (n = 6). Representative images are shown at 200- and 630-fold magnification. Data presented as median ± interquartile range. Statistical significance was determined by Mann-Whitney U-test. $P < 0.05$ was considered significant. SSc, systemic sclerosis. Color figure can be viewed in the online issue, which is available at http://onlinelibrary.wiley.com/doi/10.1002/art.43094/abstract.

enrichment with neither papillary nor reticular marker gene lists (Supplementary Figure 3B), demonstrating that this enrichment is specific for WNT/β-catenin signaling. To confirm the spatial transcriptional activity of WNT/β-catenin signaling in human skin samples, we investigated the spatial expression of the WNT/β-catenin target gene *AXIN2* using the RNAscope in situ hybridization technique (Figure 3A). As in previous studies,[25] *COL1A1* was used to identify dermal fibroblasts. Consistent with the bioinformatic analyses aforementioned, we observed significantly increased numbers of *AXIN2, COL1A1*-expressing cells in the papillary dermis compared with the reticular dermis in healthy skin. In contrast, in SSc skin, almost all *COL1A1*-expressing cells also expressed *AXIN2*, and a difference in the number of *AXIN2, COL1A1* positive cells between reticular and papillary cells was no longer detectable. The intensity of the *AXIN2* signal also demonstrated a loss of spatial expression gradients of *AXIN2* in SSc skin (Figure 3A). These results were confirmed on the protein level using immunofluorescence staining of AXIN2 in combination with the pan-fibroblast marker P4Hβ, which showed a predominance of AXIN2-positive fibroblasts in the papillary dermis of control skin. This distribution was altered in SSc skin, and comparable levels of AXIN2-positive fibroblasts were measured in both the papillary and the reticular layer of the dermis, along with a general upregulation of AXIN2 in SSc (Supplementary Figure 4).

To confirm these observations, we expanded the investigation of WNT/β-catenin-regulated genes using cyclic in situ hybridization by COSMx as an additional more comprehensive spatial transcriptomic approach. This analysis revealed that the papillary to reticular ratio of several WNT-related genes, including *CTNNB1*, *FZD1*, *FZD5*, *FZD7*, *FZD8*, *VEGFC*, *WIF1*, *WNT11*, *WNT7B*, and *FGF18*,[31–33] was found to be reduced in SSc skin fibroblasts compared with controls (Supplementary Figure 5). We also observed a tendency toward a decrease of the papillary to reticular ratio of noncanonical WNT-related genes in SSc skin, although this reduction was less pronounced compared with that seen with canonical WNT-related genes (Supplementary Figure 6).

Additionally, a distance profile analysis demonstrated that in healthy controls, fibroblasts expressing the WNT signature were located closer to the epidermis and predominantly in the papillary layer. In contrast, SSc skin showed that the WNT signature-expressing fibroblasts were more evenly distributed throughout the dermis, with similar cell densities observed in both the papillary and the reticular layer (Supplementary Figure 7). To a lesser extent, a similar distribution pattern was observed for noncanonical WNT-related genes, although the variation in localization was less pronounced (Supplementary Figure 8).

To analyze the spatial WNT activation by a complementary approach, we analyzed the spatial distribution of β-catenin expression in the skin by coimmunofluorescence staining for β-catenin and the pan-fibroblast marker P4Hβ (Figure 3B). In healthy skin, fibroblasts with nuclear β-catenin expression were enriched in the papillary dermis by two-fold compared with the reticular dermis. In SSc skin, we observed an increase of β-catenin-positive fibroblasts throughout the dermis and a particular enrichment in the papillary layer was no longer detectable (Figure 2B), showing a general overexpression of β-catenin in SSc skin fibroblasts. In noninvolved SSc skin, the distribution of β-catenin-positive fibroblasts was similar to healthy skin (Supplementary Figure 9), confirming that the disruption of the spatial distribution is inherent to fibrotic skin changes. The distribution of β-catenin-positive fibroblasts was comparable between lcSSc and dcSSc skin sections, indicating a similar pattern of spatial alteration of WNT/β-catenin signaling in both disease subtypes in involved skin (Supplementary Figure 10).

The physiologic regulation of WNT signaling relies on a controlled balance of several WNT agonists and antagonists.[9–12,14,32–35] In fact, in addition to an upregulation of WNT agonists, WNT inhibitors have been shown to be reduced in SSc skin.[14,36] We therefore analyzed the spatial distribution of the WNT antagonist DKK1 through coimmunofluorescence with the pan-fibroblast marker P4Hβ. Healthy control skin showed a predominance of DKK-positive fibroblasts in the reticular dermis. In SSc skin, we observed a significant downregulation of DKK throughout the dermis, with no differences of expression between the papillary and the reticular layer (Supplementary Figure 11).

Spatial distribution of fibroblast populations in SSc skin compared with controls. A previous study in healthy skin identified enrichment of FAP^+; $CD90^-$ fibroblasts in the papillary dermis, whereas FAP^-; $CD90^+$ fibroblasts were enriched in the reticular dermis.[37] Thus, we next analyzed whether the distribution of these two fibroblast populations in the papillary versus reticular dermis is perturbed in SSc. We observed an increase of both fibroblast populations in SSc compared with healthy controls. As analyzed by IMC and immunofluorescence, both FAP^+; $CD90^-$ fibroblasts and FAP^-; $CD90^+$ fibroblasts were increased throughout the dermis, and particular enrichment of the FAP^+; $CD90^-$ fibroblasts in the papillary dermis and FAP^-; $CD90^+$ fibroblasts in the reticular dermis was not detectable (Supplementary Figure 12).

On the transcriptomic level, fibroblast subpopulations have recently been identified based on single-cell RNA sequencing data.[27,28] We analyzed whether an enrichment of reticular marker genes is found in these populations on the transcriptomic level (Figure 4A). We observed the most pronounced enrichment of reticular genes in the PI16+ and the SFRP4+ fibroblast subsets in SSc fibroblasts compared with control fibroblasts. Next, we analyzed whether the enrichment of reticular marker genes on the transcriptomic level is also associated with the spatial redistribution of these fibroblast populations in the dermis. As analyzed by immunofluorescence staining for PI16 and SFRP4 together with the pan-fibroblast marker P4Hβ, we observed an increased

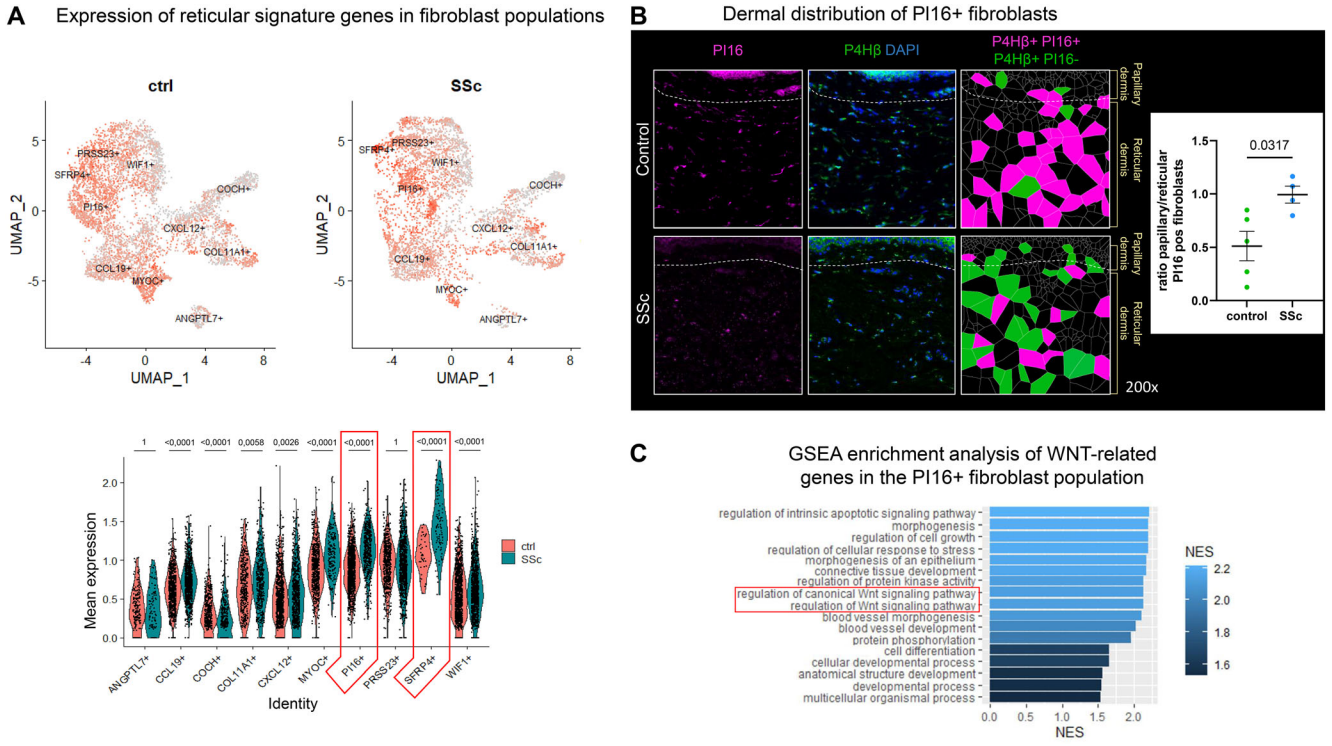

Figure 4. Analysis of fibroblast populations in relation to the papillary and reticular dermis in SSc compared with controls. (A) Mean expression of reticular marker genes in fibroblast populations defined based on small conditional RNA in SSc compared with control. Adjusted *P* values using the Bonferroni correction are shown. (B) Immunofluorescence staining for PI16 (magenta) and the pan-fibroblast marker *P4Hβ* (green) of nondiseased control individuals (n = 5) and patients with SSc (n = 4). Representative pictures are shown at 200-fold magnification. Data presented as median ± interquartile range. Statistical significance was determined by Mann-Whitney U-test. $P < 0.05$ was considered significant. (C) NES of gene sets in a PI16-positive fibroblast cluster. ctrl, control; GSEA, gene set enrichment analysis; NES, normalized enrichment score; SSc, systemic sclerosis; UMAP, uniform manifold approximation and projection. Color figure can be viewed in the online issue, which is available at http://onlinelibrary.wiley.com/doi/10.1002/art.43094/abstract.

ratio of papillary versus reticular PI16+ fibroblasts in SSc skin compared with controls (Figure 4B). In noninvolved SSc skin, the distribution of PI16-positive fibroblasts was comparable with healthy skin (Supplementary Figure 13), indicating that these changes in spatial distribution are specific to fibrotic skin alterations. The ratio of SFRP4+ fibroblasts in the papillary versus reticular dermis did not differ in SSc samples compared with healthy controls (Supplementary Figure 14).

Having demonstrated that PI16+ fibroblasts are characterized by the enrichment of reticular marker genes on the transcriptomic level and anatomically relocate to the papillary dermis in SSc, we next analyzed whether PI16+ fibroblasts also show an increased activation of WNT/β-catenin signaling. Using GSEA, we observed that gene sets associated with the regulation of WNT/β-catenin signaling are enriched in the transcriptomic profile of the PI16+ fibroblast population (Figure 4C). Similar results were obtained using Gene Ontology term analysis (Supplementary Figure 15). Consistently, coimmunofluorescence staining of β-catenin and PI16 revealed an increase of β-catenin and PI16 colocalization levels in SSc skin compared with controls (Supplementary Figure 16). In summary, these results suggest that the PI16+ fibroblasts show a particular relocation to the papillary dermis in SSc and are associated with increased WNT/β-catenin signaling.

DISCUSSION

Here we show for the first time that the physiologic gradient of WNT/β-catenin signaling is perturbed in SSc skin along with anatomic changes of the papillary and reticular dermis and with changes in the spatial distribution of specific fibroblast subsets.

In human adult healthy skin, the activation of WNT/β-catenin signaling is spatially distinct with increased activation of WNT/β-catenin signaling in the papillary dermis compared with the reticular dermis. In contrast to healthy skin, the activation of WNT/β-catenin signaling is exaggerated throughout the dermis in involved skin of patients with SSc, and the gradient of WNT/β-catenin activation between the papillary and the reticular dermis is lost. This is paralleled by a reticular skin phenotype in SSc with reduced number, size, and height of dermal papillae and the predominance of a reticular gene expression profile. Of note, PI16+ fibroblasts show a particular enrichment for both reticular marker genes and genes related to the regulation of WNT/β-catenin signaling and they are spatially enriched in the papillary dermis in SSc. These results suggest that PI16+ fibroblasts might contribute to the disruption of the skin layers in SSc.

Our findings could have potential implications for future therapeutic approaches. Dermal papillae contain sensitive skin

structures including vessels, nerve endings, mechanosensory corpuscles, hair bulbs, and skin adnexa. In addition, dermal papillae increase the skin surface and have a function in mechanotransduction themselves. Loss of the dermal papillae during fibrotic skin remodeling in SSc is thus not only associated with disrupted skin anatomy but also skin malfunction. Current state-of-the-art medications used to treat skin fibrosis mostly aim at reduction of progression of the fibrotic disease burden. Beyond that, future therapeutic approaches could aim at restoration of the normal skin structure in patients with SSc. This is further supported by a short-term clinical trial that showed that a topical WNT/β-catenin inhibitor could promote fat tissue regeneration in SSc skin,[38] suggesting that local targeting of WNT/β-catenin signaling may help to recover aspects of the physiologic tissue structure. The identification of dysregulated fibroblast populations that could specifically be targeted, whereas physiologic populations that remain unaffected might contribute to this approach. Based on our results, targeting PI16+ positive fibroblasts could be an interesting target; however, further functional experiments to better characterize this population would need to be performed as discussed in the following paragraph. Moreover, our results underline that the delicate balance of spatially distinct pathway modulation might be considered for restoring skin integrity in fibrosis disorders.

Our study has limitations. The human papillary skin structure is not sufficiently reflected in rodent skin models and advanced in vitro models showing a papillary dermis structure are not available at the time of the submission. Thus, functional experiments are limited and further studies to model the adult human dermal structure are needed to substantiate our findings.

ACKNOWLEDGMENT

Open Access funding enabled and organized by Projekt DEAL.

AUTHOR CONTRIBUTIONS

All authors contributed to at least one of the following manuscript preparation roles: conceptualization AND/OR methodology, software, investigation, formal analysis, data curation, visualization, and validation AND drafting or reviewing/editing the final draft. As corresponding author, Dr Bergmann confirms that all authors have provided the final approval of the version to be published, and takes responsibility for the affirmations regarding article submission (eg, not under consideration by another journal), the integrity of the data presented, and the statements regarding compliance with institutional review board/Declaration of Helsinki requirements.

REFERENCES

1. Gabrielli A, Avvedimento EV, Krieg T. Scleroderma. N Engl J Med 2009;360:1989–2003.
2. Decuman S, Smith V, Verhaeghe ST, Van Hecke A, De Keyser F. Work participation in patients with systemic sclerosis: a systematic review. Clin Exp Rheumatol 2014;32(6 suppl 86):S-206–S-213.
3. Wu W, Jordan S, Graf N, et al; EUSTAR Collaborators. Progressive skin fibrosis is associated with a decline in lung function and worse survival in patients with diffuse cutaneous systemic sclerosis in the European Scleroderma Trials and Research (EUSTAR) cohort. Ann Rheum Dis 2019;78:648–656.
4. Dyring-Andersen B, Løvendorf MB, Coscia F, et al. Spatially and cell-type resolved quantitative proteomic atlas of healthy human skin. Nat Commun 2020;11:5587.
5. Kanitakis J. Anatomy, histology and immunohistochemistry of normal human skin. Eur J Dermatol 2002;12:390–399.
6. Varga J, Abraham D. Systemic sclerosis: a prototypic multisystem fibrotic disorder. J Clin Invest 2007;117:557–567.
7. Van Praet JT, Smith V, Haspeslagh M, Degryse N, Elewaut D, De Keyser F. Histopathological cutaneous alterations in systemic sclerosis: a clinicopathological study. Arthritis Res Ther 2011;13:R35.
8. Montgomery H, O'Leary PA, Ragsdale WE, Jr. Dermatohistopathology of various types of scleroderma. AMA Arch Derm 1957;75:78–87.
9. Matos I, Asare A, Levorse J, et al. Progenitors oppositely polarize WNT activators and inhibitors to orchestrate tissue development. eLife 2020;9:9.
10. Akhmetshina A, Palumbo K, Dees C, et al. Activation of canonical Wnt signalling is required for TGF-β-mediated fibrosis. Nat Commun 2012;3:735.
11. Beyer C, Reichert H, Akan H, et al. Blockade of canonical Wnt signalling ameliorates experimental dermal fibrosis. Ann Rheum Dis 2013;72:1255–1258.
12. Beyer C, Schramm A, Akhmetshina A, et al. β-catenin is a central mediator of pro-fibrotic Wnt signaling in systemic sclerosis. Ann Rheum Dis 2012;71:761–767.
13. Daoussis D, Tsamandas A, Antonopoulos I, et al. B cell depletion therapy upregulates Dkk-1 skin expression in patients with systemic sclerosis: association with enhanced resolution of skin fibrosis. Arthritis Res Ther 2016;18:118.
14. Dees C, Schlottmann I, Funke R, et al. The Wnt antagonists DKK1 and SFRP1 are downregulated by promoter hypermethylation in systemic sclerosis. Ann Rheum Dis 2014;73:1232–1239.
15. Wei J, Fang F, Lam AP, et al. Wnt/β-catenin signaling is hyperactivated in systemic sclerosis and induces Smad-dependent fibrotic responses in mesenchymal cells. Arthritis Rheum 2012;64:2734–2745.
16. LeRoy EC, Black C, Fleischmajer R, et al. Scleroderma (systemic sclerosis): classification, subsets and pathogenesis. J Rheumatol 1988;15:202–205.
17. Bergmann C, Hallenberger L, Chenguiti Fakhouri S, et al. X-linked inhibitor of apoptosis protein (XIAP) inhibition in systemic sclerosis (SSc). Ann Rheum Dis 2021;80:1048–1056.
18. Bergmann C, Brandt A, Merlevede B, et al. The histone demethylase Jumonji domain-containing protein 3 (JMJD3) regulates fibroblast activation in systemic sclerosis. Ann Rheum Dis 2018;77:150–158.
19. Zehender A, Li YN, Lin NY, et al. TGFβ promotes fibrosis by MYST1-dependent epigenetic regulation of autophagy. Nat Commun 2021;12:4404.
20. Dees C, Pötter S, Zhang Y, et al. TGF-β-induced epigenetic deregulation of SOCS3 facilitates STAT3 signaling to promote fibrosis. J Clin Invest 2020;130:2347–2363.
21. Ashhurst TM, Marsh-Wakefield F, Putri GH, et al. Integration, exploration, and analysis of high-dimensional single-cell cytometry data using Spectre. Cytometry A 2022;101:237–253.
22. Eling N, Damond N, Hoch T, Bodenmiller B. Cytomapper: an R/Bioconductor package for visualization of highly multiplexed imaging data. Bioinformatics 2020;36:5706–5708.
23. Györfi AH, Matei AE, Fuchs M, et al. Engrailed 1 coordinates cytoskeletal reorganization to induce myofibroblast differentiation. J Exp Med 2021;218:e20201916.

24. Solé-Boldo L, Raddatz G, Schütz S, et al. Single-cell transcriptomes of the human skin reveal age-related loss of fibroblast priming. Commun Biol 2020;3:188.
25. Skaug B, Khanna D, Swindell WR, et al. Global skin gene expression analysis of early diffuse cutaneous systemic sclerosis shows a prominent innate and adaptive inflammatory profile. Ann Rheum Dis 2020; 79:379–386.
26. Assassi S, Sharif R, Lasky RE, et al; GENISOS Study Group. Predictors of interstitial lung disease in early systemic sclerosis: a prospective longitudinal study of the GENISOS cohort. Arthritis Res Ther 2010;12:R166.
27. Tabib T, Huang M, Morse N, et al. Myofibroblast transcriptome indicates SFRP2^{hi} fibroblast progenitors in systemic sclerosis skin. Nat Commun 2021;12:4384.
28. Zhu H, Luo H, Skaug B, et al. Fibroblast subpopulations in systemic sclerosis: functional implications of individual subpopulations and correlations with clinical features. J Invest Dermatol 2024;144:1251–1261.e13.
29. Fuchs E. Keratins and the skin. Annu Rev Cell Dev Biol 1995;11: 123–153.
30. Wei J, Melichian D, Komura K, et al. Canonical Wnt signaling induces skin fibrosis and subcutaneous lipoatrophy: a novel mouse model for scleroderma? Arthritis Rheum 2011;63:1707–1717.
31. Ramakrishnan AB, Cadigan KM. Wnt target genes and where to find them. F1000Res 2017;6:746.
32. MacDonald BT, Tamai K, He X. Wnt/beta-catenin signaling: components, mechanisms, and diseases. Dev Cell 2009;17:9–26.
33. Nusse R, Clevers H. Wnt/beta-catenin signaling, disease, and emerging therapeutic modalities. Cell 2017;169:985–999.
34. Bergmann C, Distler JH. Canonical Wnt signaling in systemic sclerosis. Lab Invest 2016;96:151–155.
35. Dees C, Distler JH. Canonical Wnt signalling as a key regulator of fibrogenesis - implications for targeted therapies? Exp Dermatol 2013;22:710–713.
36. Henderson J, Pryzborski S, Stratton R, O'Reilly S. Wnt antagonist DKK-1 levels in systemic sclerosis are lower in skin but not in blood and are regulated by microRNA33a-3p. Exp Dermatol 2021;30: 162–168.
37. Korosec A, Frech S, Gesslbauer B, et al. Lineage identity and location within the dermis determine the function of papillary and reticular fibroblasts in human skin. J Invest Dermatol 2019;139:342–351.
38. Lafyatis R, Mantero JC, Gordon J, et al. Inhibition of β-catenin signaling in the skin rescues cutaneous adipogenesis in systemic sclerosis: a randomized, double-blind, placebo-controlled trial of C-82. J Invest Dermatol 2017;137:2473–2483.